ADVANCED ELECTRONIC MATERIALS
www.advelectronicmat.de

Check for updates

Multifunctional Graphene Composites for Electromagnetic Shielding and Thermal Management at Elevated Temperatures

Zahra Barani, Fariborz Kargar, Amirmahdi Mohammadzadeh, Sahar Naghibi, Carissa Lo, Brandon Rivera, and Alexander A. Balandin**

A method for scalable synthesis of epoxy composites with graphene and few-layer graphene fillers is described, and the electromagnetic interference (EMI) shielding and thermal properties of such composites at elevated temperatures are reported. The tested materials reveal excellent total EMI shielding of $SE_T \approx 65$ dB (≈ 105 dB) at a thickness of 1 mm (≈ 2 mm) in the X-band frequency range. At higher filler loading fractions, composites reveal a room-temperature cross-plane thermal conductivity of 11.2 ± 0.9 $Wm^{-1} K^{-1}$, which is a factor of ×41 larger than that of the pristine epoxy. Interestingly, the EMI shielding efficiency improves further as the temperature increases while the thermal conductivity remains approximately constant. The enhancement in the EMI shielding is explained by the temperature dependence of the two electrical conduction mechanisms, electronic band-type conduction inside the fillers, and hopping conduction between the fillers. The excellent EMI shielding and heat conduction characteristics of such multifunctional graphene composites at high temperatures are promising for packaging applications of microwave components where EMI shielding and thermal management are important design considerations.

1. Introduction

Rapid miniaturization and a consequent increase in the heat and electromagnetic wave (EM) emission in the densely-packed electronic systems make the simultaneous heat management and electromagnetic interference (EMI) shielding crucially important.[1–3] Any working electronic device is the source of EM radiation. For this reason, the electronic components have to be protected from the intra- and inter-system EM radiations in order to avoid fast degradation and failure.[4–14] It has also been suggested that prolonged exposure to even non-ionizing EM waves in the MHz and GHz frequency range may have detrimental effects on humans and other living beings making the EMI shielding important from safety perspectives.[15–19] The dense packing of the electronic components in the state-of-the-art 2D, 2.5D, and 3D integrated systems and generation of high heat fluxes create an environment with high temperatures, which adversely affect the efficiency and stability of the EMI shielding materials.[20,21] The absorption of EM waves results in the temperature rise of the material making the situation even worse. The data on the efficiency of the conventional and recent EM shield materials in most cases are limited to room temperature (RT) operation.[20–23] The latter is despite the fact that many new non-metallic materials, introduced for EMI shielding, suffer from thermal instability, oxidation, or significant reduction in the shielding efficiency at high temperatures. These concerns require development of novel multifunctional materials, which can serve concurrently as an excellent EM shields with the high thermal stability and conductivity at elevated temperatures. The ability of such materials to act as the thermal interface materials (TIMs) which can dissipate heat efficiently becomes a necessity rather than an extra bonus feature.[2,3,20,21,24] TIMs are applied between two solid surfaces in order to fill the microscopic voids at the interface, and enhance the thermal transport from a heat source to a heat sink.[25–27] The base materials for TIMs are amorphous polymers, which have low thermal conductivity, typically in the range from 0.2 to 0.5 $Wm^{-1} K^{-1}$.[28] For this reason, the polymers used as base materials for TIMs are filled with highly thermally conductive fillers to enhance their overall thermal conductivity. The low-weight, mechanical stability, resistance to oxidation, flexibility, and ease of manufacturing are other important criteria for TIMs.

EMI shielding materials block the incident EM waves by reflection and absorption mechanisms. Both mechanisms

Z. Barani, Prof. F. Kargar, A. Mohammadzadeh, S. Naghibi, C. Lo, Prof. A. A. Balandin
Phonon Optimized Engineered Materials (POEM) Center
Materials Science and Engineering Program
University of California
Riverside, CA 92521, USA
E-mail: fkargar@engr.ucr.edu; balandin@ece.ucr.edu

Z. Barani, Prof. F. Kargar, A. Mohammadzadeh, B. Rivera, Prof. A. A. Balandin
Nano-Device Laboratory (NDL)
Department of Electrical and Computer Engineering
Bourns College of Engineering
University of California
Riverside, CA 92521, USA

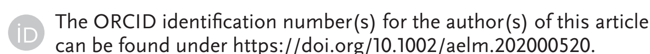
The ORCID identification number(s) for the author(s) of this article can be found under https://doi.org/10.1002/aelm.202000520.

DOI: 10.1002/aelm.202000520

 © 2020 Wiley-VCH GmbH

require interaction of the EM waves with the charge carriers in the material. For this reason, EMI shielding materials should be either electrically conductive or contain electrically conductive fillers. Nonetheless, high electrical conductivity is not a requirement for EMI shielding and bulk resistivity on the order of 1 Ω cm is sufficient for the most industrial applications.[4,14,29] The conventional materials used for EMI shielding are metals, which are utilized as coatings and enclosures.[20,29] Metals possess a high density of mobile charge carriers, which blocks the EM waves mostly by the reflection mechanism.[23] Metallic shields are heavy and prone to oxidation, resulting in corrosion. The electrical conductivity of metals and, correspondingly, shielding efficiency are degraded at high temperatures.[30,31] An alternative approach is utilization of polymers filled with high loadings of metallic particles. Although the polymer-metal composites alleviate the problems associated with corrosion and oxidation, they suffer from heavy weight and degraded efficiency at elevated temperatures.[31,32] Ceramics,[33–40] carbon fibers,[41–48] carbon black,[49,50] carbon nanotubes,[51–57] graphite,[58–60] reduced graphene oxide,[5,8,61–71] graphene,[72–76] ferromagnetic materials,[77–80] and combinations of carbon allotropes with metallic and nonmetallic fil lers[69,71,72,74,81–86] have been tested as potential fillers for EMI shielding applications. Ceramic fillers have demonstrated a promise for high-temperature applications owing to their excellent thermal stability and relatively high thermal conductivity at high temperatures. However, ceramic materials are electrical insulators and do not absorb well the EM waves in the microwave spectral region.[20] Carbon allotropes such as graphene and carbon nanotubes demonstrated better performance as fillers in polymeric matrices. Other advantages of carbon fillers include the low weight, high thermal stability, and anti-corrosive properties.[20,57,87] Among all fillers mentioned previously, graphene and few-layer graphene (FLG) have both high electrical conductivity and the highest thermal conductivity.[88–93] From the fundamental science point of view, graphene is more compatible with the polymeric matrices than carbon nanotubes owing to its 2D nature. Technologically, graphene can be mixed and processed more conveniently without agglomeration and better coupling to the matrix material. Composites filled with ceramics and other carbon allotropes exhibit lower thermal conductivity comparing to that of graphene. A new type of metallic fillers, MXenes, demonstrated high EMI shielding efficiency in the X-band frequency range.[4] However, these materials are prone to oxidation, particularly at increased temperatures, limiting their stability and EM shielding applications.[94,95] The in-plane thermal conductivity of MXene films is reported to be ≈ 3 to ≈ 4 Wm^{-1} K^{-1}, substantially lower than that of graphene-based composite materials.[96]

The intrinsic thermal conductivity of graphene is in the range of 2000–5000 Wm^{-1} K^{-1} depending on its lateral dimensions, crystal quality, and defect concentration.[91–93] For practical thermal applications, a mixture of graphene and FLG is the most beneficial because FLG retains the excellent heat conduction properties while offering higher cross-section area for the heat flux. Owing to their mechanical flexibility, graphene fillers facilitate the formation of the interconnected network of FLG fillers. Phonons are the main heat carriers in graphene and FLG. For this reason, large lateral dimensions of the fillers are required in order to preserve the heat conduction properties.[97] The phonon mean free path (MFP) in graphene is ≈ 750–800 nm, suggesting that the fillers used in composites should have lateral dimensions exceeding the phonon MFP.[98] The thermal transport properties of FLG are expected to be less affected by the exposure to the matrix material. In our recent study, we reported an enhancement of the thermal conductivity by a factor of × 51 at $\varphi = 45$ vol% loading fraction of a mixture of graphene and FLG.[26] The thermal conductivity of ≈ 15 Wm^{-1} K^{-1} can now be routinely reached by an addition of graphene fillers to polymer matrices.[99–101] The thermal conductivity enhancement factor depends on the quality of the filler, its average lateral dimension, and the composite synthesis procedure.

Despite the importance of knowing EMI shielding efficiency at elevated temperatures and thermal properties of EMI composites, there have been few studies that provided such data. Here, we report on the EMI shielding properties and thermal characteristics of the multifunctional epoxy—based composites with FLG fillers which also demonstrates the excellent high-temperature performance of such materials. The composites exhibit room temperature cross-plane thermal conductivity of 11.2 ± 0.9 Wm^{-1} K^{-1} and the total shielding efficiency of 65 dB at a thickness of $t = 1$ mm at the filler loading of $\varphi = 19.5$ vol% in the X-band frequency range of $f = 8.2$ GHZ − 12.4 GHz. The EMI shielding and thermal properties of the samples were examined at the temperatures beyond 500 K. The results show that the graphene—epoxy samples preserve their excellent heat conduction properties at high temperatures while the EMI shielding efficiency even improves. The excellent EMI shielding and thermal properties of the multi-functional graphene composites at elevated temperatures along with their thermal stability and light-weight are important for electronic packaging and airborne systems where efficient EMI shielding, low cost, and low weight are required at high temperatures and high power densities.

2. Material Synthesis and Characterization

The materials synthesis processes and quality control steps for epoxy-based composites with graphene and FLG fillers are illustrated in **Figure 1**a–e. The samples were synthesized with the commercially available graphene powder (xGnP, grade H, XG-Sciences, USA) and epoxy resin (bisphenol-A-(epichlorhydrin), molecular weight ≤700, Allied High-Tech Products, Inc.) and hardener (triethylenetetramine, Allied High Tech Products, Inc.). It has been shown that graphene fillers with a larger aspect ratio provide the highest EMI shielding efficiency and thermal conductivity.[2,26,102–106] This explains the selection of the graphene powder with the largest average lateral dimensions of the flakes. A representative scanning electron microscopy (SEM) image of FLG utilized in the composite preparation confirming their large lateral dimensions in the range of 15–25 µm is shown in Figure S1a,b, Supporting Information. In order to prepare composites with different filler concentrations, FLG powder was added to epoxy resin in certain amounts, followed by the addition of the hardener. The compound was mixed using a high shear speed mixer (Flacktek Inc) in several steps

© 2020 Wiley-VCH GmbH

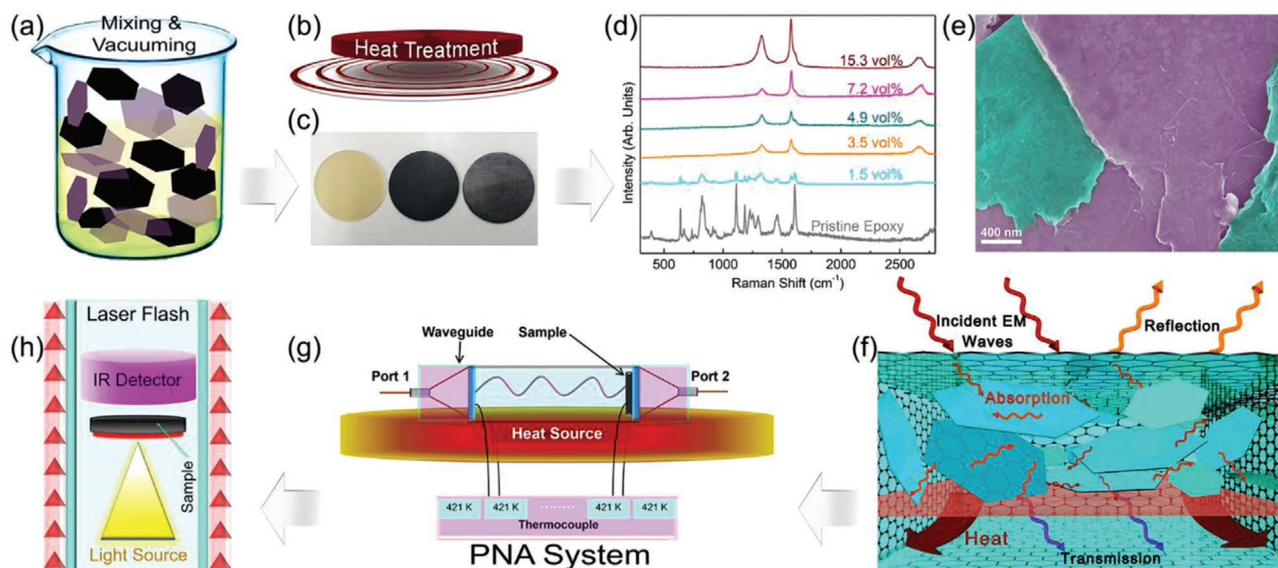

Figure 1. Process flow for the sample preparation and characterization. a) Mixing and vacuuming FLG with the epoxy resin and hardener. The mixture is left to solidify for ≈8 h at RT. b) Heat treatment of the cured samples at 120 °C for ≈1 h. c left to right) Optical image of a pristine epoxy sample, and an epoxy sample with 11.4 vol% and 15.3 vol% loading of FLG. d) Raman spectra of epoxy with various FLG filler loadings. e) SEM image of a composite with 15.3 vol% of FLG fillers, revealing filler overlapping inside the matrix. f) Schematic showing the interaction of the EM waves with the composite. g) Schematic of the experimental setup for the temperature dependent EMI shielding measurements, and h) schematic of the laser flash system used for thermal conductivity measurements.

to obtain a uniform dispersion. The mixture was vacuumed several times at least for 15 min at each step in order to remove any possible voids or air bubbles. The final mixture was poured into round molds, gently pressed, and left to solidify at RT for ≈8 h. After curing, the samples were placed in a furnace for ≈1 h at 120 °C (Figure 1a,b). It should be noted that in the EMI shielding experiments, the thickness of the sample affects its absorption and thus, its total shielding efficiency. Therefore, for detailed comparison, all samples were polished down to the same thickness of ≈ 1.00 mm. An optical image of the pristine epoxy and the composite with 11.4 vol% and 15.3 vol% of graphene fillers is shown in Figure 1c.

The quality of the samples was verified by the SEM inspection and Raman spectroscopy. Raman spectra of representative samples with different graphene loadings are shown in Figure 1d. The intensity of the characteristic Raman peaks of graphene, namely the G peak at ≈ 1580 cm^{-1} and 2D band at 2700 cm^{-1}, increases as more graphene is loaded to the epoxy. These two peaks are not distinguishable in the samples with graphene loading less than $\varphi \leq 1.5$ vol%. The variations in the graphene filler concentration and their overlap are clearly seen in the SEM image of the composite with 15.3 vol% of the fillers (see Figure 1e). Additional data of SEM inspection of the samples are provided in Figure S1c–f, Supporting Information. The data confirms that at high loadings, graphene fillers overlap forming the electrically percolated networks. The filler attachments and percolation strongly affects the electrical and thermal characteristics of the composites, and finally their EMI shielding performance at RT and above. The process of EM wave interaction with the graphene composite is illustrated in Figure 1f. Large hexagons indicate FLG fillers. A fraction of the incident EM wave is reflected at the air-composite interface. A part of the EM wave, which passes through the composite's interface, is absorbed directly or after multiple internal reflections inside the composite. Only a small fraction of the incident EM wave is transmitted through the samples. The absorption of EM waves results in the increase of the composite's temperature, which explains the need for high thermal conductivity of EMI shielding material. In the schematic, the red arrows indicate the highly conductive paths for heat dissipation through the fillers inside the epoxy polymer base. The EMI shielding efficiency and the cross-plane thermal conductivity of the samples were measured using a programmable network analyzer (PNA) (see Figure S2, Supporting Information) and a "laser flash" instrument (see Figure S3, Supporting Information). The schematic and operational principles of both systems are shown in Figure 1g,h. The details of the experimental setups and measurements are provided in the Experimental Section and Supporting Information.

3. Results and Discussion

3.1. Electromagnetic Interference Shielding

To determine EMI characteristics, we measured the scattering parameters, S_{ij}, using the two-port PNA system at RT and higher temperatures. The indices i and j represents the ports, which are receiving and emitting the EM waves. Each port can simultaneously emit and detect the EM waves and thus, the results of the measurements include four parameters of S_{11}, S_{12}, S_{21}, and S_{22}. Given that the samples are symmetric, one can expect that $|S_{11}| = |S_{22}|$ and $|S_{12}| = |S_{21}|$. The scattering parameters are related to the coefficients of reflection, $R = |S_{11}|^2$, and

 © 2020 Wiley-VCH GmbH

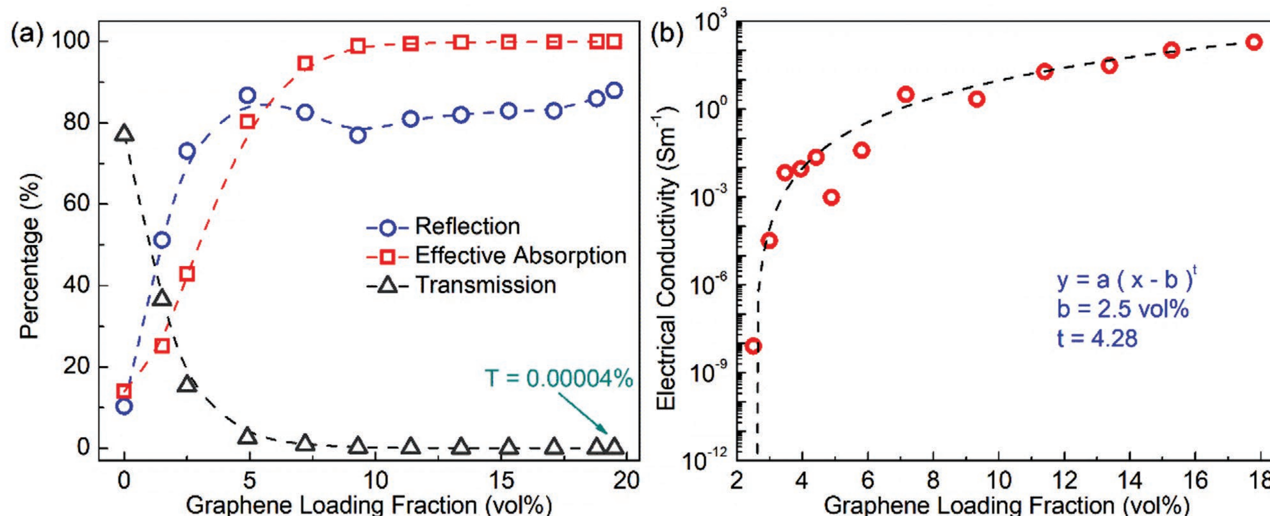

Figure 2. a) Coefficients of reflection (R), effective absorption (A_{eff}), and transmission (T) as a function of filler loading at $f = 9.0$ GHz. The rate of variation of R, A_{eff}, and T becomes smaller for $\varphi > 2.5$ vol%. b) Bulk in-plane electrical conductivity versus filler loading. The electrical percolation threshold is extracted at $\varphi_e = 2.5$ vol% via fitting the experimental data using $\sigma \approx (\varphi - \varphi_{th})^t$.

transmission, $T = |S_{21}|^2$.[107] Knowing these two coefficients, one can obtain the coefficient of absorption, A, according to $A = 1 - R - T$. This is because for any EM wave incident on the sample, a fraction is reflected at the interface. A part of EM wave, which enters the composite, is absorbed and the rest is transmitted. The coefficient of absorption, which is defined as the power percentile of the absorbed EM wave in the medium to the total power of incident wave, is not truly indicative of material's ability in absorbing the EM waves since some part of the wave is reflected at the interface prior to entering the medium. For this reason, the effective absorption coefficient, A_{eff}, is defined as $A_{eff} = (1 - R - T)/(1 - R)$. After determining R, T, and A_{eff}, the shielding efficiency of the material can be calculated.

Figure 2a shows the coefficients of R, A_{eff}, and T of the epoxy composites as a function of graphene loading fraction at a representative frequency of $f = 9$ GHz. The main observation is that addition of even small loading of graphene results in rapid increase in the reflection and effective absorption, and a corresponding decrease in transmission. For the filler concentrations greater than $\varphi > 2.5$ vol%, the rate of change for all three coefficients becomes small. The reflection increases from ≈ 10% for pristine epoxy to ≈ 85% for the samples with $\varphi \geq 4.9\%$ and remains constant with negligible variations at higher loading fractions. The effective absorption exhibits a similar trend, showing an abrupt increase from 42% at $\varphi = 2.5$ vol% to 80% at $\varphi = 4.9\%$, and an asymptotical approach to 100% at the higher loadings. At a high loading of $\varphi = 19.5$ vol%, the blocking of EM waves by reflection and absorption becomes so strong that only 0.00004% of the incident wave is transmitted through the medium (Figure 2a, black triangles). The calculated R, T, A and A_{eff} as a function of the frequency for the samples with different FLG concentrations are presented in Figure S4, Supporting Information.

The attenuation of EM waves in a conductive medium is related to the skin depth, δ.[107] In good conductors, $\delta = (\pi f \mu \sigma)^{-1/2}$ where f, μ, and σ are the EM wave frequency, medium's permeability, and electrical conductivity, respectively. Graphene and FLG are good conductors of electricity. The sheet resistance of SLG and FLG vary from ≈100 Ω to 30 kΩ depending on the number of layers and quality.[88–90] Pristine epoxy, on the other hand, is an electrical insulator with the conductivity in the order of ≈ 10^{-16} Sm^{-1}.[108] Addition of FLG to the epoxy, increases the composite's electrical conductivity after the establishment of the percolation network of the fillers. The results of the standard room-temperature four-probe in-plane electrical conductivity measurements of the epoxy with FLG as a function of the filler loading are presented in Figure 2b. The details of the measurements are explained in the Experimental Section and Supporting Information. The abrupt change in conductivity observed at $\varphi = 2.5$ vol% indicates the onset of the electrical percolation where the large FLG fillers inside the insulating polymer matrix create an electrically conductive network. Electrical percolation is theoretically described by power scaling law, $\sigma \approx (\varphi - \varphi_e)^t$, where φ_e is the filler loading fraction at the electrical percolation threshold, and t is the "universal" critical exponent.[102,109] The coincidence of the electrical percolation threshold shown in Figure 2b and the filler loading at which the abrupt change in the effective absorption and transmission is observed demonstrate the correlation among these parameters.

The total shielding efficiency, SE_{tot}, describes the total attenuation of the incident EM wave as it hits and passes through the composite. This parameter determines the material's ability to block the EM waves and consists of two terms of reflection loss, or reflection shielding efficiency, SE_R, and absorption loss, or absorption shielding efficiency, SE_A. These parameters can be calculated in terms of R, T, and A_{eff} as follows:[2,107]

$$SE_R = 10\log\left[\left(P_i/(P_i - P_r\right)\right] = -10\log(1-R) \tag{1}$$

$$SE_A = 10\log\left[\left(P_i - P_r\right)/\left(P_i - P_r - P_a\right)\right] = -10\log(1-A_{eff}) \tag{2}$$

 © 2020 Wiley-VCH GmbH

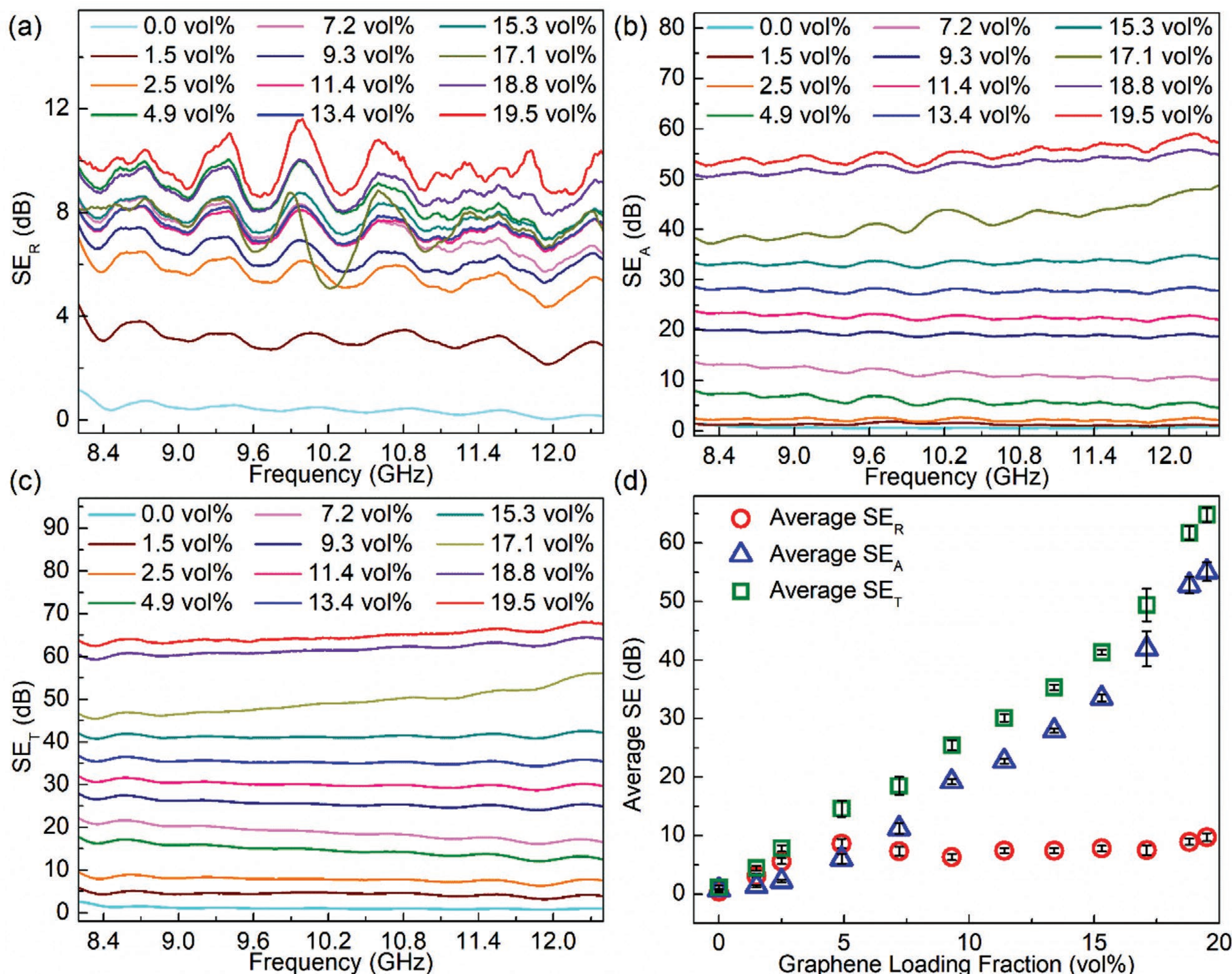

Figure 3. a) Reflection (SE_R), b) absorption (SE_A), and c) total EMI shielding efficiency (SE_T) of the composite of 1 mm thickness in the frequency range from 8.0 to 12.4 GHz at different graphene loading fractions. With the increasing graphene loading, the EMI shielding efficiency of the composites improves significantly. The total EMI shielding of the composites reaches to ≈65 dB at 19.5 vol% of the graphene filler concentration. d) Average reflection (red circles), absorption (blue triangles), and total EMI shielding (green squares) of composites over the entire X-band frequency range as a function of graphene loading.

$$SE_T = 10\log\left(P_i/P_t\right) = SE_R + SE_A \quad (3)$$

where P_i, P_r, P_a, and P_t are the power of incident, reflected, absorbed, and transmitted EM wave, respectively.

Figure 3a–c shows SE_R, SE_A, and SE_T of the samples as the functions of the graphene filler loading. As more fillers are loaded to the pristine epoxy polymer, SE_R rapidly increases (Figure 3a). At $\varphi \geq 2.5$ vol%, the enhancement in reflection becomes slower, and the SE_R saturates, that is, it does not increase significantly with more graphene loading. The reflection efficiency is directly related to the surface electrical conductivity or, in other words, the concentration of free charge carriers at or near the interface. The saturation behavior of SE_R indicates that the large graphene fillers are overlapping at the surface of the sample, increasing the overall electrical conductivity of the sample by orders of magnitude as compared to that of pristine epoxy or composites with low loading. Note that at $\varphi = 2.5$ vol%, $R \approx 73\%$ indicating that most part of the incident EM wave is already reflected back at the interface. In contrast, SE_A increases with adding more fillers (Figure 3b). In samples with $\varphi \geq 2.5$ vol%, the absorption loss becomes the dominant shielding mechanism. This can be seen clearly at higher filler loadings where SE_A approaches 52 dB at $\varphi = 19.5$ vol% meaning that almost all the remaining fraction of the EM wave, which passes through the medium after reflection, is being absorbed by the composites. Figure 3c presents the total EMI shielding efficiency of the samples as a function of the graphene loading. The average reflection, absorption, and total shielding efficiency of composites over the complete X-band frequency range as a function of graphene loading are shown in Figure 3d. As it is seen and described previously, the reflection loss (red circles) initially increases but then saturates and becomes almost constant at $\varphi \geq 2.5$ vol% whereas the absorption and thus, total shielding efficiency continue to increase with addition of more fillers. One can summarize the difference in behavior by noting that reflection is mostly a

 © 2020 Wiley-VCH GmbH

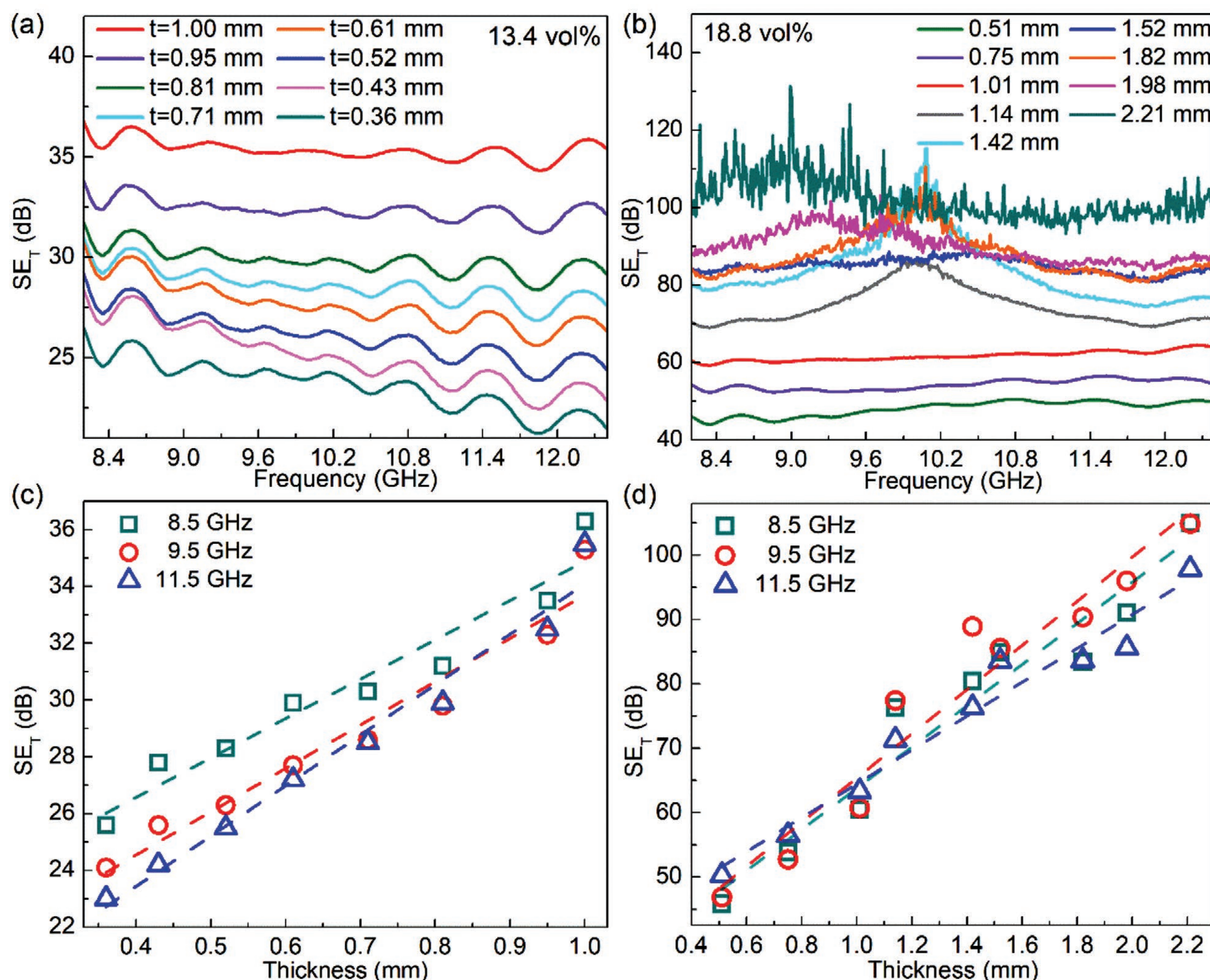

Figure 4. Total EMI shielding of epoxy composites with a) 13.4 vol% and b) 18.8 vol% graphene filler loading as a function of frequency at different thicknesses. Total EMI shielding of the epoxy composites with c) 13.4 vol% and d) 18.8 vol% loading of the filler versus the thickness of the composites at frequencies of 8.5, 9.5, and 11.5 GHz. Note that the EM shielding increases linearly with increasing the thickness of the composite owing to the increase in shielding by absorption.

surface phenomenon while absorption happens in the volume of the composite. The electrically conducting percolation network forms at the surface at lower graphene loading than in the volume of the material.

In **Figure 4**a,b we present the EMI shielding efficiency as a function of the thickness for the epoxy composites with 13.4 vol% and 18.8 vol% graphene loading, respectively. The absorption shielding efficiency is directly related to the thickness of the sample. The classical Simon's equation relates the SE_A to the thickness according to $SE_A = (1.7t/\rho)f^{0.5}$ where t [cm] and ρ [Ωcm] are the sample's thickness and bulk DC resistivity and f [MHz] is the frequency. With the increasing thickness, the SE_A increases, which results in the enhancement of the total EMI shielding efficiency (see Eq. (3)). The dependence of SE_T as a function of the sample's thickness is shown in Figure 4c,d for the composites with 13.4 vol% and 18.8 vol% at the fixed frequencies of 8.5 GHz, 9.5 GHz, and 11.5 GHz. The dashed lines are the fitted linear regression over the experimental data. A clear linear trend is observable in both panels. It should be noted that for the epoxy composite with graphene loading of 18.8 vol% and thickness of ≈ 2 mm, the total shielding efficiency at different frequencies is between 95 dB to 105 dB. The values achieved in our samples exceed the EMI shielding requirements for most industrial applications, which are at the level of the total 30 dB shielding efficiency.[2,29] Another advantage of the graphene-enhanced epoxy composites is that they provide higher EM shielding at much lower weights and with stable mechanical structure as compared to conventional metallic enclosures, which are widely used in electronic packaging.

Densely packed electronics, in addition to emitting undesirable EM waves to the environment, dissipate high amounts of heat, which leads to the increase in temperature of all components in the electronic package. A part of the EM wave, which turns into heat during the absorption process, can be described by the following equation:[20]

$$P = \frac{1}{2}\sigma|E|^2 + \pi f\varepsilon_0\varepsilon_r''|E|^2 + \pi f\mu_0\mu_r''|H|^2 \quad (4)$$

© 2020 Wiley-VCH GmbH

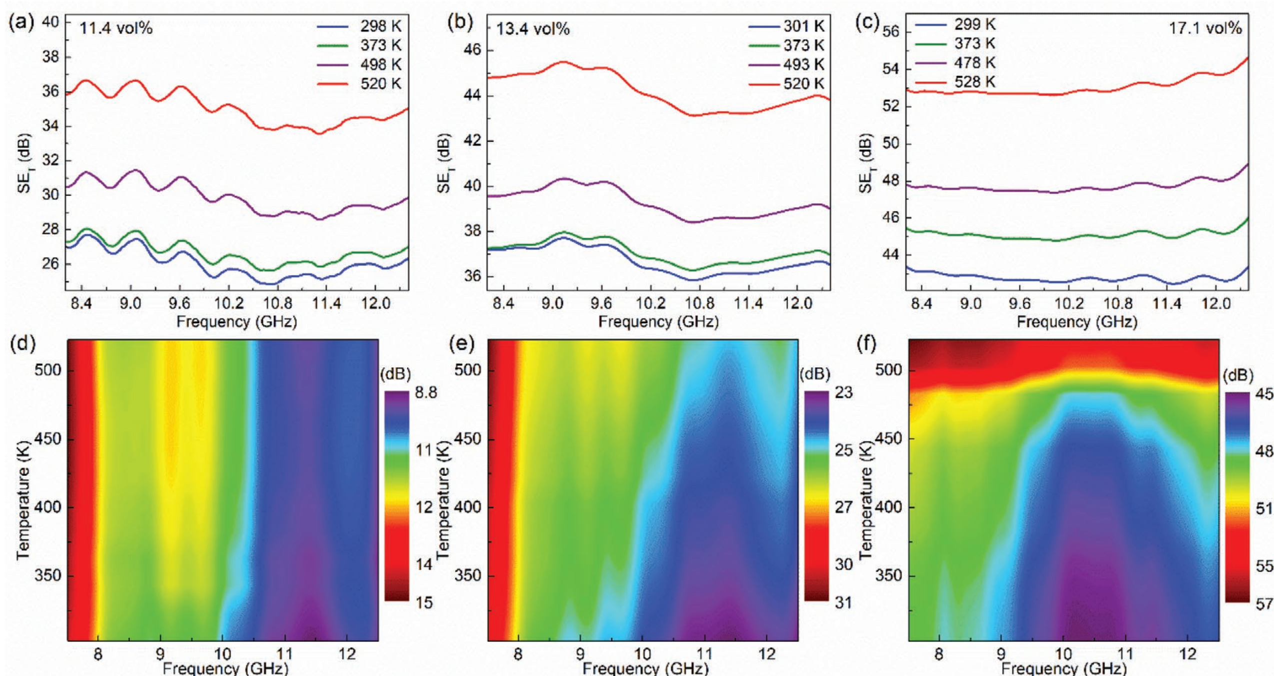

Figure 5. Total EMI shielding efficiency of the epoxy with a) 11.4 vol%, b) 13.4 vol%, and c) 17.1 vol% of graphene fillers as a function of temperature in the X-band frequency range. The EMI efficiency increases with temperature in all samples. The color map of the total EMI shielding efficiency of the composites with d) 3.5 vol%, e) 9.3 vol%, and f) 17.1 vol% of graphene loading filler loading as a function of frequency in the temperature range from 303 K to 523 K The EMI attenuation for all samples increase as the temperature rises. The enhancement is more pronounced at higher frequencies.

Here, P is the power, ε_0 and ε''_r are the vacuum and imaginary part of medium's relative permittivity, and μ_0 and μ''_r are the vacuum and imaginary part of medium's relative permeability. The first, second, and the third terms in the right hand side correspond to the Joule heat loss, dielectric loss, and magnetic loss, where the latter is negligible for the epoxy composites with graphene. The temperature-rise in most cases adversely affect the ability of materials in blocking the EM waves. In this regard, the EM shield material must possess a high thermal stability, that is, preserving its EM shielding characteristics even at elevated temperatures at least up to 500 K, and relatively high thermal conductivity in order to dissipate heat to the environment.

Figure 5a–c shows the EM shielding efficiency of three composites with 11.4 vol%, 13.4 vol%, and 17.1 vol% graphene loading at four selected temperatures, in the temperature range from 298 to 528 K. The total shielding efficiency of the samples enhances by ≈ 8 dB for all filler loadings as the temperature increases from RT to ≈ 520 K. In Figure 5d–f, we present color maps of SE_T as the function of temperature and frequency for composites with the low (3.5 vol%), medium (9.3 vol%), and high (17.1 vol%) graphene loadings. In contrast to some prior studies, we observed a continuous increase in the SE_T for all filler loadings.[32,110] The increase in the SE_T is originated mainly from the enhancement in absorption loss rather than increase in the reflection attenuation (see Figure S5, Supporting Information). The epoxy composites reach the electrical percolation threshold at a rather low FLG concentration of $\varphi \approx 2.5$ vol%. In these samples, the absorption is defined by the electrical conductivity. In a disordered system of randomly dispersed FLG fillers in a polymer matrix, the conductivity by migrating electrons (σ_m) in the plane of FLG fillers and conductivity by hopping electrons (σ_h) among the different FLG fillers affect the bulk average electrical conductivity of the composite. The hopping conductance mechanism is generally described as $\sigma_h \approx e^{-(T_0/T)^p}$ where T_0 depends on the material's property and p is a parameter defined by the type of hopping. As the temperature increases, the hopping conductivity strongly increases. One should note that the electrical conductivity in graphite and graphene also increases with temperature rise.[110,111] For these reasons, both mechanisms of electrical conduction in epoxy-graphene composites enhance with increasing temperature. The latter explains the increase in the absorption and the EMI shielding efficiency at elevated temperatures.

The high thermal stability of epoxy composites laden with FLG fillers provides several advantages over other types of EM shielding materials and fillers, that is, ceramics, ferromagnets, or MXenes. Ceramic-based composites usually use SiC, which, although thermally stable, has rather poor absorption properties. The ferromagnetic fillers lose their magnetic properties as the temperature passes the Curie temperature, causing the drop in their magnetic shielding characteristics at elevated temperatures. The MXene fillers and films exhibit high shielding efficiencies but prone to formation of oxide layers and reveal poor thermal conductivity making them unsuitable for high-temperature EMI shielding applications.[76,94–96,112]

 © 2020 Wiley-VCH GmbH

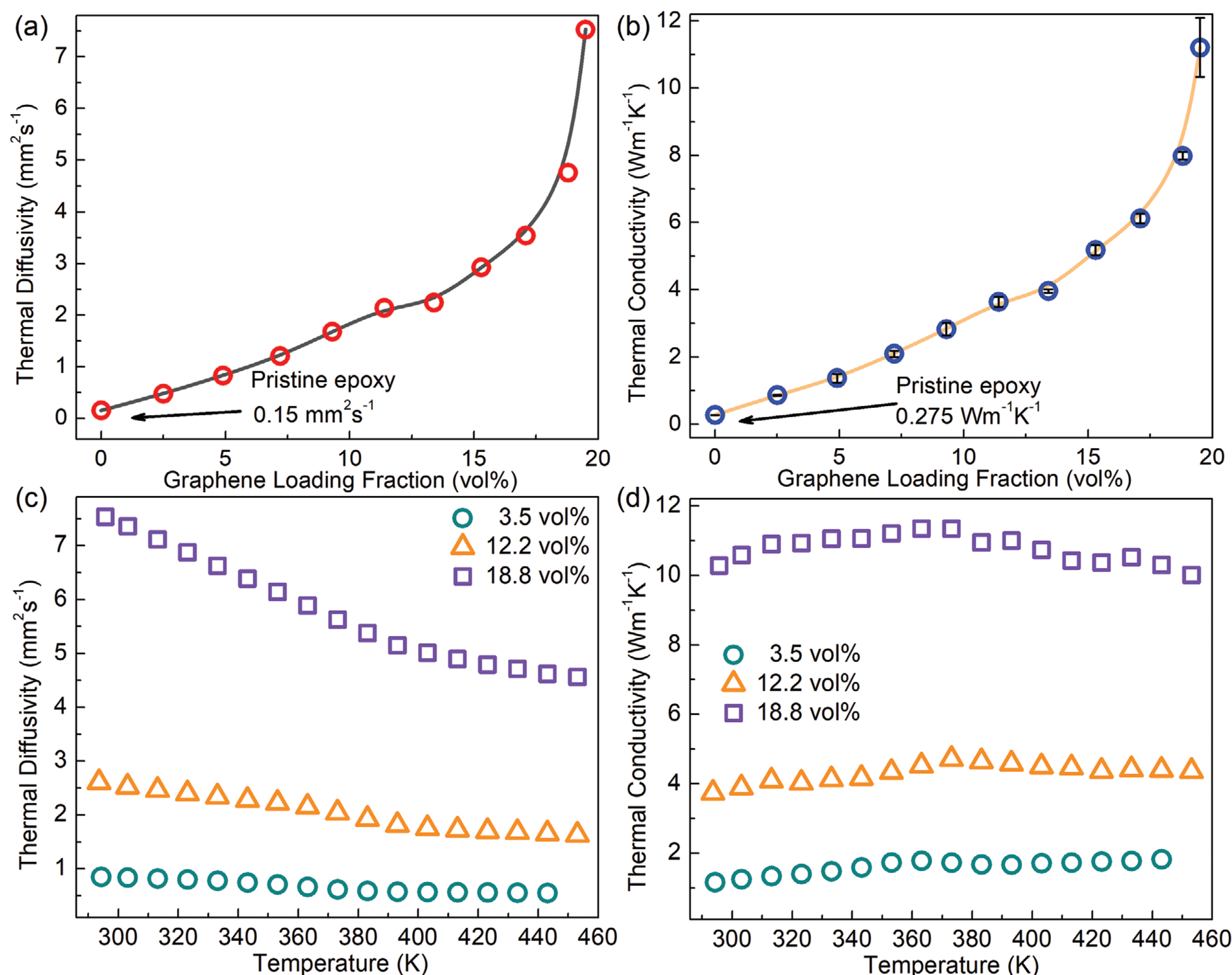

Figure 6. Thermal properties of the graphene composites. a) Thermal diffusivity and b) thermal conductivity of the composites as a function of graphene loading fraction at room temperature. The thermal conductivity exhibits a quadratic dependence on the filler loading except near the loading $\varphi \approx$ 11.4 vol% where there is plateau-like dependence attributed to the formation of graphene clusters. (c) Thermal diffusivity and d) thermal conductivity of three different composites with the low, medium, and high loading of graphene fillers as a function of temperature. The thermal diffusivity decreases with temperature. The thermal conductivity remains nearly constant because the increase in the specific heat compensates for the decrease in thermal diffusivity as the temperature rises.

3.2. Thermal Characteristics

The cross-plane thermal diffusivity and conductivity of the composites at RT and at elevated temperatures were measured using the "laser flash" analysis (LFA, 467 HyperFlash, NETZSCH, Germany). The schematic and operational principal of the measurements are shown in Figure 1h. The thermal diffusivity, α, was measured directly while the thermal conductivity, K, was calculated as $K = \rho\alpha c_p$, where ρ and c_p are the mass density and the specific heat. The density of the composites was measured using the Archimedes principle. The specific heat was measured by LFA instrument. The details of the experimental setup and measurements are provided in the Experimental Section. **Figure 6**a,b shows the cross-plane thermal diffusivity and thermal conductivity of the composites as the functions of the graphene loading. Both thermal characteristics, α and K, grow fast with increasing graphene loading. The super-linear, nearly of higher than quadratic, dependence of the thermal characteristics of the composites as the function of the filler loading is attributed to creation of the highly thermally conductive paths of the percolated FLG fillers. The mechanism of the thermal percolation in epoxy composites with graphene has been described by us previously.[26,99,113] One should note that epoxy composites with only 19.5 vol% FLG loading provide cross-plane thermal conductivity of 11.2 ± 0.9 Wm^{-1} K^{-1}, which is comparable to that of the ceramic materials, widely used in high–temperature EMI shielding, specifically for their rather high thermal conductivity and thermal stability. The advantages of graphene composites over conventional ceramics are much higher EMI shielding efficiency at much lower weights.

In order to investigate the thermal stability of the composites, we carried out temperature dependent thermal diffusivity

© 2020 Wiley-VCH GmbH

and conductivity experiments in the temperature range between RT to 460 K. the results of the measurements are presented in Figure 6c,d. The thermal diffusivity of the samples decreases with increasing the temperature. The rate of change is more significant for the composites with higher graphene loadings. However, the thermal conductivity is almost constant owing to the increase in the specific heat as the temperature increases (Figure S6, Supporting Information). One should note that the reported data is for the thermal transport properties in the cross-plane direction. The in-plane thermal conductivity of the samples is expected to be much higher because graphene flakes tend to align in the in-plane direction during the fabrication process.[101] The nearly constant high thermal conductivity of the composites over a wide temperature range demonstrates that epoxy with graphene fillers can serve as a multifunctional composite for applications in electronic systems, providing excellent EMI shielding, heat dissipation, mechanical support and adhesion even at elevated temperatures.

4. Conclusions

We examined the EMI shielding efficiency and thermal conductivity of multi-functional epoxy composites with graphene fillers at elevated temperatures. It was found that graphene composites with the filler loading of $\varphi = 19.5$ vol% exhibit a high total shielding efficiency of 65 dB at a thickness of 1 mm in the X-band frequency range. The same composite reveals high thermal conductivity of 11.2 ± 0.9 Wm^{-1} K^{-1} at RT. The composites preserve their high thermal conductivity at elevated temperatures while their EMI shielding efficiency increases for all examined filler loadings. The excellent EMI shielding and heat conduction properties of graphene composites are important for the thermal management and electromagnetic compatibility of the next generation of high-power, high-temperature electronic devices where the weight, cost, and functionality at harsh environments are of utmost importance.

5. Experimental Section

Sample Preparation: The samples were prepared by mixing the commercially available FLG flakes (xGnP graphene nanoplatelets, grade H, XG-Sciences) with epoxy (Allied High Tech Products, Inc.). For samples with less than 15 vol% loading fraction of FLG, the epoxy resin and the filler were mixed using a high-shear speed mixer (Flacktek Inc.) at 800 and 2000 rpm each for 5 min. The mixture was vacuumed for 10 min at least three times. At the end, the curing agent (Allied High Tech Products, Inc.) was added in the mass ratio of 12:100 with respect to the epoxy resin. The mixture was mixed and vacuumed one more time and left in the room temperature for 8 h to be cured. The prepared composite samples were put in the furnace for ≈1 h at 120 °C in order to solidify. For samples with more than 15 vol% loading fraction of FLG, there were two additional steps. First, the solution was mixed at high rotation speeds of 3000 for 10 to15 s while adding graphene to the resin at the beginning of the procedure. At the end, the homogenous mixture was gently pressed before being left to cure. The details of the sample preparation are provided in the Supporting Information. The graphene volume fraction of the samples was calculated according to the composite rule of mixtures as $\varphi = V_f/V_c = (m_f/\rho_f)/(m_f/\rho_f + m_e/\rho_e)$. In this formula, m, V, and ρ are the mass fraction, volume, and density of the composite's constituents. The subscripts f, e, and c represents "filler," "epoxy," and "composite," respectively.

Electromagnetic Interference Shielding Measurements: RF measurements were performed in the X-Band frequency range (8.2 − −12.4 GHz) with frequency resolution of 3 MHz at RT and elevated temperatures. A PNA Keysight N5221A was used. The PNA was calibrated for 2-port measurements of scattering parameters S_{ij} at input power $P_{in} = 3$ dBm. A WR-90 commercial grade straight waveguide with two adapters at both ends with SMA coaxial ports was used as a sample holder. In order to carry out high-temperature RF measurements, the waveguide with the sample were heated using a hot-plate heater. The temperature of the waveguide and the samples were measured using 6 thermocouples attached at different points of the waveguide (see Figure 1g). Prior to collecting the temperature dependent RF measurements, the waveguide without any samples was tested in the temperature range between RT and 520 K. The performance of the waveguide did not change with temperature rise. Figure S7, Supporting Information, shows the SE_T of the bare waveguide without any samples as a function of temperature. Special cables were used for high temperature RF measurements. The samples with diameter $d \geq 25$ mm were a bit larger than the rectangular cross section (22.8×10.1 mm^2) of the central hollow part of the waveguide in order to prevent the leakage of EM waves from the sender to receiver antenna. The scattering parameters, S_{ij}, were directly measured and used to extract the reflection and absorption shielding efficiency of the composites.

Electrical Conductivity Measurements: The in-plane DC resistance and conductivity of the graphene composites with the FLG fillers using standard 4-probe configuration. For this purpose, four needles contacted the surface of the sample using the probe station. The schematic and experimental setup of the measurements are shown in Figure S8, Supporting Information. The distance between the contacts was ≈ 5 mm. The current was applied to the outer contacts and the voltage difference was measured between the two inner contacts. The resistivity was calculated, according to $\rho = GV/I$, where G is the geometrical factor and V and I are the measured voltage and applied current. The geometrical factor can be calculated according to $G = \frac{\pi}{Ln2} t T_2 \frac{t}{s}$ where t is the thickness of the samples and s is the distance between two adjacent contacts. The coefficient T_2 is the correction factor extracted from the standard plots. If $\frac{t}{s} \ll 1$, one can assume that $T_2 t/s \rightarrow 1$ and thus, $G = 4.5324t$.[114] The conductivity is calculated as $\sigma = 1/\rho$.

Mass Density Measurements: According to Archimedes principle and by using an electronic scale (Mettler Toledo), the mass density of the samples was measured. In this method the density is defined using $\rho_c = (w_a/(w_a - w_w)) \times (\rho_w - \rho_a) + \rho_a$ formula where w_a, w_w are the sample's weight in air and in water and ρ_w and ρ_a are the density of the ionized water and air (0.0012 gcm^{-3}) at room temperature.

Thermal Diffusivity, Specific Heat Capacity, and Thermal Conductivity Measurements: Thermal diffusivity of the samples were measured using the transient "laser flash" technique (LFA 467 HyperFlash, NETZSCH) compliant with the international standards of ASTM E-1461, DIM EN 821 and DIN 30 905. The heat capacity is calculated based on comparison of the temperature rise of the sample with that of the known reference sample. Later on the values off thermal diffusivity obtained directly from LFA, were used to determine the thermal conductivity value of the samples. Knowing the density, thermal diffusivity, and the specific heat of the sample, thermal conductivity was calculated according to the equation $K = \rho \alpha c_p$ where K, ρ, and c_p are the thermal conductivity, density, and specific heat, respectively. In LFA technique, the front surface of a plane-parallel sample was heated by a short energy pulse. From the resulting temperature excursion of the rear face measured with an infrared (IR) detector, the thermal diffusivity was obtained. More details on the LFA thermal conductivity method can be found in Supporting Information.

 © 2020 Wiley-VCH GmbH

Supporting Information

Supporting Information is available from the Wiley Online Library or from the author.

Acknowledgements

The work at UCR was supported, in part, by the Office of Technology Partnerships (OTP), University of California via the Proof of Concept (POC) project "Graphene Thermal Interface Materials." A.A.B. also acknowledges the UC—National Laboratory Collaborative Research and Training Program—University of California Research Initiatives LFR-17-477237. The authors acknowledge useful discussions on EM measurements with Dr. Alexander Khitun (UC Riverside) and thank Alec Balandin (Riverside STEM Academy) for assistance with the composite preparations and Raman measurements.

Conflict of Interest

The authors declare no conflict of interest.

Author Contributions

A.A.B., F.K., and Z.B. conceived the idea of the study. A.A.B. and F.K. coordinated the project and contributed to the experimental and theoretical data analysis. Z.B. prepared the composites, performed thermal and EMI shielding measurements, and conducted data analysis. A.M. contributed to the sample characterization; S.N., C.L., and B.R. assisted with sample preparation; Z.B. and F.K. led the manuscript preparation. All authors contributed to writing and editing of the manuscript.

Keywords

electromagnetic interference shielding, graphene, high-temperature electronics, thermal conductivity, thermal management

Received: May 20, 2020
Revised: August 13, 2020
Published online:

[1] C. Liang, K. Ruan, Y. Zhang, J. Gu, *ACS Appl. Mater. Interfaces* **2020**, *12*, 18023.
[2] F. Kargar, Z. Barani, M. Balinskiy, A. S. Magana, J. S. Lewis, A. A. Balandin, *Adv. Electron. Mater.* **2019**, *5*, 1800558.
[3] Y. Guo, L. Pan, X. Yang, K. Ruan, Y. Han, J. Kong, J. Gu, *Composites, Part A* **2019**, *124*, 105484.
[4] F. Shahzad, M. Alhabeb, C. B. Hatter, B. Anasori, S. Man Hong, C. M. Koo, Y. Gogotsi, *Science* **2016**, *353*, 1137.
[5] Z. Chen, C. Xu, C. Ma, W. Ren, H.-M. Cheng, *Adv. Mater.* **2013**, *25*, 1296.
[6] N. Yousefi, X. Sun, X. Lin, X. Shen, J. Jia, B. Zhang, B. Tang, M. Chan, J.-K. Kim, *Adv. Mater.* **2014**, *26*, 5480.
[7] B. Shen, W. Zhai, W. Zheng, *Adv. Funct. Mater.* **2014**, *24*, 4542.
[8] D.-X. Yan, H. Pang, B. Li, R. Vajtai, L. Xu, P.-G. Ren, J.-H. Wang, Z.-M. Li, *Adv. Funct. Mater.* **2015**, *25*, 559.
[9] X. Zhang, X. Zhang, M. Yang, S. Yang, H. Wu, S. Guo, Y. Wang, *Compos. Sci. Technol.* **2016**, *136*, 104.
[10] X.-H. Li, X. Li, K.-N. Liao, P. Min, T. Liu, A. Dasari, Z.-Z. Yu, *ACS Appl. Mater. Interfaces* **2016**, *8*, 33230.
[11] B. Shen, Y. Li, D. Yi, W. Zhai, X. Wei, W. Zheng, *Carbon* **2016**, *102*, 154.
[12] P. Kumar, F. Shahzad, S. Yu, S. M. Hong, Y.-H. H. Kim, C. M. Koo, *Carbon* **2015**, *94*, 494.
[13] M.-S. Cao, X.-X. Wang, W.-Q. Cao, J. Yuan, *J. Mater. Chem. C* **2015**, *3*, 6589.
[14] D. D. Chung, *Carbon* **2001**, *39*, 279.
[15] F. Deruelle, *Electromagn. Biol. Med.* **2020**, *39*, 166.
[16] R. N. Kostoff, P. Heroux, M. Aschner, A. Tsatsakis, *Toxicol. Lett.* **2020**, *323*, 35.
[17] M. H. Repacholi, *Bioelectromagnetics* **1998**, *19*, 1.
[18] A. Zamanian, C. Hardiman, *High Freq. Electron.* **2005**, *4*, 16.
[19] L. Hardell, C. Sage, *Biomed. Pharmacother.* **2008**, *62*, 104.
[20] J. P. Gogoi, A. Shabir, in *Materials for Potential EMI Shielding Applications* (Eds: J. Kuruvilla, W. Runcy, G. Gejo), Elsevier, Amsterdam **2020**, pp. 379–390.
[21] Z. Jia, K. Lin, G. Wu, H. Xing, H. Wu, *Nano* **2018**, *13*, 1830005.
[22] D. Wanasinghe, F. Aslani, G. Ma, D. Habibi, *Nanomaterials* **2020**, *10*, 541.
[23] D. Jiang, V. Murugadoss, Y. Wang, J. Lin, T. Ding, Z. Wang, Q. Shao, C. Wang, H. Liu, N. Lu, R. Wei, A. Subramania, Z. Guo, *Polym. Rev.* **2019**, *59*, 280.
[24] C. Liang, M. Hamidinejad, L. Ma, Z. Wang, C. B. Park, *Carbon* **2020**, *156*, 58.
[25] F. P. Incropera, D. P. DeWitt, T. L. Bergman, A. S. Lavine, *Introduction to Heat Transfer*, 6th ed., John Wiley & Sons, Weinheim, Germany **2007**.
[26] F. Kargar, Z. Barani, R. Salgado, B. Debnath, J. S. Lewis, E. Aytan, R. K. Lake, A. A. Balandin, *ACS Appl. Mater. Interfaces* **2018**, *10*, 37555.
[27] S. Naghibi, F. Kargar, D. Wright, C. Y. T. Huang, A. Mohammadzadeh, Z. Barani, R. Salgado, A. A. Balandin, *Adv. Electron. Mater.* **2020**, *6*, 1901303.
[28] X. Xie, D. Li, T.-H. Tsai, J. Liu, P. V. Braun, D. G. Cahill, *Macromolecules* **2016**, *49*, 972.
[29] R. M. Simon, *Polym. Plast. Technol. Eng.* **1981**, *17*, 1.
[30] R. A. Matula, *J. Phys. Chem. Ref. Data* **1979**, *8*, 1147.
[31] T. Merizgui, A. Hadjadj, B. Gaoui, M. Kious, in *Proc. 2018 Int. Conf. Applied Smart Systems (ICASS)*, Institute Of Electrical And Electronics Engineers Inc., Medea, Algeria **2018**, pp. 1–5.
[32] B. Wen, M. Cao, M. Lu, W. Cao, H. Shi, J. Liu, X. Wang, H. Jin, X. Fang, W. Wang, J. Yuan, *Adv. Mater.* **2014**, *26*, 3484.
[33] X. Yin, L. Kong, L. Zhang, L. Cheng, N. Travitzky, P. Greil, *Int. Mater. Rev.* **2014**, *59*, 326.
[34] M. Li, X. Yin, G. Zheng, M. Chen, M. Tao, L. Cheng, L. Zhang, *J. Mater. Sci.* **2015**, *50*, 1478.
[35] H. J. Yang, W. Q. Cao, D. Q. Zhang, T. J. Su, H. L. Shi, W. Z. Wang, J. Yuan, M. S. Cao, *ACS Appl. Mater. Interfaces* **2015**, *7*, 7073.
[36] Y. Wang, F. Luo, P. Wei, W. Zhou, D. Zhu, *J. Electron. Mater.* **2015**, *44*, 2353.
[37] Q. Yuchang, W. Qinlong, L. Fa, Z. Wancheng, *J. Mater. Chem. C* **2016**, *4*, 4853.
[38] C. Luo, T. Jiao, J. Gu, Y. Tang, J. Kong, *ACS Appl. Mater. Interfaces* **2018**, *10*, 39307.
[39] Y. Tan, H. Luo, X. Zhou, S. Peng, H. Zhang, *Sci. Rep.* **2018**, *8*, 2915.
[40] A. Plyushch, J. MacUtkevic, S. Svirskas, J. Banys, V. Plausinaitiene, D. Bychanok, S. A. Maksimenko, A. Selskis, A. Sokal, K. N. Lapko, P. P. Kuzhir, *Appl. Phys. Lett.* **2019**, *114*, 183105.
[41] W.-L. Song, J. Wang, L.-Z. Fan, Y. Li, C.-Y. Wang, M.-S. Cao, *ACS Appl. Mater. Interfaces* **2014**, *6*, 10516.
[42] Y. Yang, M. C. Gupta, K. L. Dudley, *Nanotechnology* **2007**, *18*, 345701.
[43] Y. Yang, M. C. Gupta, K. L. Dudley, R. W. Lawrence, *Adv. Mater.* **2005**, *17*, 1999.
[44] A. Ameli, P. U. Jung, C. B. Park, *Carbon* **2013**, *60*, 379.

 © 2020 Wiley-VCH GmbH

[45] B. O. Lee, W. J. Woo, H. S. Park, H. S. Hahm, J. P. Wu, M. S. Kim, *J. Mater. Sci.* **2002**, *37*, 1839.
[46] M. Bayat, H. Yang, F. K. Ko, D. Michelson, A. Mei, *Polymer* **2014**, *55*, 936.
[47] M. Crespo, N. Méndez, M. González, J. Baselga, J. Pozuelo, *Carbon* **2014**, *74*, 63.
[48] J. Wu, Z. Ye, H. Ge, J. Chen, W. Liu, Z. Liu, *J. Colloid Interface Sci.* **2017**, *506*, 217.
[49] S. Mondal, S. Ganguly, P. Das, D. Khastgir, N. C. Das, *Composites, Part B* **2017**, *119*, 41.
[50] S. Kuester, C. Merlini, G. M. O. Barra, J. C. Ferreira, A. Lucas, A. C. de Souza, B. G. Soares, *Composites, Part B* **2016**, *84*, 236.
[51] M. H. Al-Saleh, U. Sundararaj, *Carbon* **2009**, *47*, 1738.
[52] Y. Yang, M. C. Gupta, K. L. Dudley, R. W. Lawrence, *Nano Lett.* **2005**, *5*, 2131.
[53] N. C. Das, Y. Liu, K. Yang, W. Peng, S. Maiti, H. Wang, *Polym. Eng. Sci.* **2009**, *49*, 1627.
[54] A. Kausar, S. Ahmad, S. M. Salman, *Polym. Plast. Technol. Eng.* **2017**, *56*, 1027.
[55] J.-M. Thomassin, C. Jérôme, T. Pardoen, C. Bailly, I. Huynen, C. Detrembleur, *Mater. Sci. Eng., R* **2013**, *74*, 211.
[56] J.-H. Lin, Z.-I. Lin, Y.-J. Pan, C.-L. Huang, C.-K. Chen, C.-W. Lou, *Composites, Part B* **2016**, *89*, 424.
[57] D. D. L. Chung, *Carbon* **2012**, *50*, 3342.
[58] G. De Bellis, A. Tamburrano, A. Dinescu, M. L. Santarelli, M. S. Sarto, *Carbon* **2011**, *49*, 4291.
[59] V. Panwar, R. M. Mehra, *Polym. Eng. Sci.* **2008**, *48*, 2178.
[60] X. Jiang, D.-X. Yan, Y. Bao, H. Pang, X. Ji, Z.-M. Li, *RSC Adv.* **2015**, *5*, 22587.
[61] J. Ling, W. Zhai, W. Feng, B. Shen, J. Zhang, W. G. Zheng, *ACS Appl. Mater. Interfaces* **2013**, *5*, 2677.
[62] S.-T. Hsiao, C.-C. M. Ma, W.-H. Liao, Y.-S. Wang, S.-M. Li, Y.-C. Huang, R.-B. Yang, W.-F. Liang, *ACS Appl. Mater. Interfaces* **2014**, *6*, 10667.
[63] D.-X. Yan, P.-G. Ren, H. Pang, Q. Fu, M.-B. Yang, Z.-M. Li, *J. Mater. Chem.* **2012**, *22*, 18772.
[64] B. Yuan, L. Yu, L. Sheng, K. An, X. Zhao, *J. Phys. D: Appl. Phys.* **2012**, *45*, 235108.
[65] B. Yuan, C. Bao, X. Qian, L. Song, Q. Tai, K. M. Liew, Y. Hu, *Carbon* **2014**, *75*, 178.
[66] B. Wen, X. X. Wang, W. Q. Cao, H. L. Shi, M. M. Lu, G. Wang, H. B. Jin, W. Z. Wang, J. Yuan, M. S. Cao, *Nanoscale* **2014**, *6*, 5754.
[67] J. Liang, Y. Wang, Y. Huang, Y. Ma, Z. Liu, J. Cai, C. Zhang, H. Gao, Y. Chen, *Carbon* **2009**, *47*, 922.
[68] J. Dalal, S. Lather, A. Gupta, S. Dahiya, A. S. Maan, K. Singh, S. K. Dhawan, A. Ohlan, *Compos. Sci. Technol.* **2018**, *165*, 222.
[69] A. Mazzoli, V. Corinaldesi, J. Donnini, C. Di Perna, D. Micheli, A. Vricella, R. Pastore, L. Bastianelli, F. Moglie, V. M. Primiani, *J. Build. Eng.* **2018**, *18*, 33.
[70] W. Yang, Z. Zhao, K. Wu, R. Huang, T. Liu, H. Jiang, F. Chen, Q. Fu, *J. Mater. Chem. C* **2017**, *5*, 3748.
[71] F. Sharif, M. Arjmand, A. A. Moud, U. Sundararaj, E. P. L. Roberts, *ACS Appl. Mater. Interfaces* **2017**, *9*, 14171.
[72] F. Ren, D. Song, Z. Li, L. Jia, Y. Zhao, D. Yan, P. Ren, *J. Mater. Chem. C* **2018**, *6*, 1476.
[73] B. Shen, Y. Li, D. Yi, W. Zhai, X. Wei, W. Zheng, *Carbon* **2017**, *113*, 55.
[74] B. Zhao, C. Zhao, R. Li, S. M. Hamidinejad, C. B. Park, *ACS Appl. Mater. Interfaces* **2017**, *9*, 20873.
[75] Y. Li, B. Shen, D. Yi, L. Zhang, W. Zhai, X. Wei, W. Zheng, *Compos. Sci. Technol.* **2017**, *138*, 209.
[76] Q. Wei, S. Pei, X. Qian, H. Liu, Z. Liu, W. Zhang, T. Zhou, Z. Zhang, X. Zhang, H. Cheng, W. Ren, *Adv. Mater.* **2020**, *32*, 1907411.
[77] Y. Li, X. Fang, M. Cao, *Sci. Rep.* **2016**, *6*, 24837.
[78] J. Liu, M. S. Cao, Q. Luo, H. L. Shi, W. Z. Wang, J. Yuan, *ACS Appl. Mater. Interfaces* **2016**, *8*, 22615.
[79] V. Sharma, J. Saha, S. Patnaik, B. K. Kuanr, *J. Magn. Magn. Mater.* **2017**, *439*, 277.
[80] Y. Zhou, W. Zhou, Y. Qing, F. Luo, D. Zhu, *J. Magn. Magn. Mater.* **2015**, *374*, 345.
[81] B. Zhao, S. Wang, C. Zhao, R. Li, S. M. Hamidinejad, Y. Kazemi, C. B. Park, *Carbon* **2018**, *127*, 469.
[82] Y. Zhan, J. Wang, K. Zhang, Y. Li, Y. Meng, N. Yan, W. Wei, F. Peng, H. Xia, *Chem. Eng. J.* **2018**, *344*, 184.
[83] Z. Min, H. Yang, F. Chen, T. Kuang, *Mater. Lett.* **2018**, *230*, 157.
[84] S.-H. Lee, D. Kang, I.-K. Oh, *Carbon* **2017**, *111*, 248.
[85] M. Verma, S. S. Chauhan, S. K. Dhawan, V. Choudhary, *Composites, Part B* **2017**, *120*, 118.
[86] Q. Song, F. Ye, X. Yin, W. Li, H. Li, Y. Liu, K. Li, K. Xie, X. Li, Q. Fu, L. Cheng, L. Zhang, B. Wei, *Adv. Mater.* **2017**, *29*, 1701583.
[87] S. Geetha, K. K. S. Kumar, C. R. K. Rao, M. Vijayan, D. C. Trivedi, *J. Appl. Polym. Sci.* **2009**, *112*, 2073.
[88] X. Li, G. Zhang, X. Bai, X. Sun, X. Wang, E. Wang, H. Dai, *Nat. Nanotechnol.* **2008**, *3*, 538.
[89] G. Liu, S. Rumyantsev, M. S. Shur, A. A. Balandin, *Appl. Phys. Lett.* **2013**, *102*, 093111.
[90] K. Nagashio, T. Nishimura, K. Kita, A. Toriumi, *Appl. Phys. Express* **2009**, *2*, 025003.
[91] A. A. Balandin, S. Ghosh, W. Bao, I. Calizo, D. Teweldebrhan, F. Miao, C. N. Lau, *Nano Lett.* **2008**, *8*, 902.
[92] W. Cai, A. L. Moore, Y. Zhu, X. Li, S. Chen, L. Shi, R. S. Ruoff, *Nano Lett.* **2010**, *10*, 1645.
[93] A. A. Balandin, *Nat. Mater.* **2011**, *10*, 569.
[94] C. J. Zhang, S. Pinilla, N. McEvoy, C. P. Cullen, B. Anasori, E. Long, S. H. Park, A. Seral-Ascaso, A. Shmeliov, D. Krishnan, C. Morant, X. Liu, G. S. Duesberg, Y. Gogotsi, V. Nicolosi, *Chem. Mater.* **2017**, *29*, 4848.
[95] T. Habib, X. Zhao, S. A. Shah, Y. Chen, W. Sun, H. An, J. L. Lutkenhaus, M. Radovic, M. J. Green, *npj 2D Mater. Appl.* **2019**, *3*, 8.
[96] L. Chen, X. Shi, N. Yu, X. Zhang, X. Du, J. Lin, *Materials* **2018**, *11*, 1701.
[97] S. Ghosh, W. Bao, D. L. Nika, S. Subrina, E. P. Pokatilov, C. N. Lau, A. A. Balandin, *Nat. Mater.* **2010**, *9*, 555.
[98] S. Ghosh, I. Calizo, D. Teweldebrhan, E. P. Pokatilov, D. L. Nika, A. A. Balandin, W. Bao, F. Miao, C. N. Lau, *Appl. Phys. Lett.* **2008**, *92*, 151911.
[99] Z. Barani, A. Mohammadzadeh, A. Geremew, C. Y. Huang, D. Coleman, L. Mangolini, F. Kargar, A. A. Balandin, *Adv. Funct. Mater.* **2020**, *30*, 1904008.
[100] M. Shtein, R. Nadiv, M. Buzaglo, K. Kahil, O. Regev, *Chem. Mater.* **2015**, *27*, 2100.
[101] A. Ohayon-Lavi, M. Buzaglo, S. Ligati, S. Peretz-Damari, G. Shachar, N. Pinsk, M. Riskin, Y. Schatzberg, I. Genish, O. Regev, *Carbon* **2020**, *163*, 333.
[102] S. Stankovich, D. A. Dikin, G. H. B. Dommett, K. M. Kohlhaas, E. J. Zimney, E. A. Stach, R. D. Piner, S. B. T. Nguyen, R. S. Ruoff, *Nature* **2006**, *442*, 282.
[103] P. Bonnet, D. Sireude, B. Garnier, O. Chauvet, *Appl. Phys. Lett.* **2007**, *91*, 201910.
[104] Z. Ounaies, C. Park, K. E. Wise, E. J. Siochi, J. S. Harrison, *Compos. Sci. Technol.* **2003**, *63*, 1637.
[105] M. Foygel, R. D. Morris, D. Anez, S. French, V. L. Sobolev, *Phys. Rev. B: Condens. Matter Mater. Phys.* **2005**, *71*, 104201.
[106] W. Bauhofer, J. Z. Kovacs, *Compos. Sci. Technol.* **2009**, *69*, 1486.
[107] M. N. O. Sadiku, *Elements of Electromagnetics*, 3rd ed., Oxford University Press, Oxford **2005**.
[108] S. Singha, M. Thomas, *IEEE Trans. Dielectr. Electr. Insul.* **2008**, *15*, 12.

© 2020 Wiley-VCH GmbH

[109] H. Pang, T. Chen, G. Zhang, B. Zeng, Z.-M. Li, *Mater. Lett.* **2010**, *64*, 2226.
[110] M.-S. S. Cao, W.-L. L. Song, Z.-L. L. Hou, B. Wen, J. Yuan, *Carbon* **2010**, *48*, 788.
[111] W. Q. Cao, X. X. Wang, J. Yuan, W. Z. Wang, M. S. Cao, *J. Mater. Chem. C* **2015**, *3*, 10017.
[112] R. Kang, Z. Zhang, L. Guo, J. Cui, Y. Chen, X. Hou, B. Wang, C. Te Lin, N. Jiang, J. Yu, *Sci. Rep.* **2019**, *9*, 9135.
[113] J. S. Lewis, Z. Barani, A. S. Magana, F. Kargar, A. A. Balandin, *Mater. Res. Express* **2019**, *6*, 085325.
[114] D. K. Schroder, *Semiconductor Material and Device Characterization*, John Wiley & Sons, Weinheim, Germany **2015**.

© 2020 Wiley-VCH GmbH